# Compensation for transient chamber wall condition using real-time plasma density feedback control in an inductively coupled plasma etcher

Pete I. Klimecky, J. W. Grizzle, and Fred L. Terry, Jr.

Department of Electrical Engineering and Computer Science, University of Michigan,

1301 Beal Ave., Ann Arbor, MI 48109-2122

ABSTRACT

Reactive ion etch processing is known to exhibit significant variability in final etch performance due to wall condition. Previous studies have shown that neutral species transients depend strongly upon chamber seasoning. In this paper, we show the first reported simultaneous measurements of wall-state-induced changes in plasma density and poly-Si etch rate, and demonstrate a real-time feedback control system that corrects for the plasma density variation. We demonstrate that controlling the plasma density to constant value eliminates the classic "first wafer effect" in $Cl_2$ etching of poly-Si in a Lam 9400 TCP. Chamber conditions studied include fluorination/cleaning by $C_2F_6$ plasmas compared to chlorination/deposition from $Cl_2$ plasmas. Transient density changes due to wall condition were measured using a microwave resonance cavity technique called BroadBand RF. Following chamber fluorination, BroadBand data show a significant drop in electron density (~39%) from nominal levels. This is followed by subsequent partial recovery of the nominal density during a 60 s $Cl_2$ etch. Independent measurements correlate strongly with the BroadBand signals; particularly real-time poly-Si etch rate and $SiCl_4$ etch product concentration. Observed real-time variations in all signals were then compensated using a single input/single output (SISO) proportional-

integral (PI) feedback control algorithm, in which the BroadBand peak frequency is the system output variable and TCP power is the system actuator. Such PI control not only stabilizes BroadBand peak frequencies, but also steadies poly-Si real-time etch rate and $SiCl_4$ etch product concentration. This compensation scheme is then applied over multiple runs to reduce etch depth variability due to chamber condition. Results of this control system are shown to attenuate first wafer effects by a factor of three and reduce overall etch depth variation from run to run by an additional 33% compared to standard manufacturing practice. When applied to patterned wafer etches, feedback control of plasma density with an oxide hardmask is found not to alter critical dimensions or profile in any observable way. Only total etch depth appears to be affected using density control, as the real-time etch rate is in general increased in comparison to open-loop etching.

PACS codes: 85.40.-e, 85.40.Hp, 52.70.-m

## I. INTRODUCTION

High yield, high throughput processing is of primary importance in modern semiconductor manufacturing. With critical dimensions (CD) approaching 100 nm and below, the demand for consistent reactive ion etching (RIE) steps is crucial to increasing overall yield while maintaining high wafer throughput. Although many advances have been made to this end, some of the most useful plasma chemistries ($Cl_2$ in particular) and process regimes (high density and low pressure) are highly complex, non-linear systems which are incompletely modeled. Modern RIE processing requires multiple test wafers,

frequent plasma clean steps, and frequent chamber maintenance in order to reduce variance and maintain a consistent manufacturing environment. Tighter controls on the root causes of etch variance would therefore tighten fabrication tolerances and improve overall equipment efficiency (OEE).

An area of current interest regarding the source of process variations over time is that of the process chamber wall condition.[1,2,3,4,5,6,7] Experimental measurements of neutral atomic Cl concentration ($n_{Cl}^{0}$) transients and correlations of these transients with chamber conditions have previously been reported.[1-4,7] In addition to neutral reactive species variations with wall state, other authors have demonstrated average etch rate changes corresponding to the chamber seasoning.[8,4] Different rate limiting reactions at the wall surface have been proposed as reasons for changes in $n_{Cl}^{0}$ concentrations, dependent upon whether an $SiO_2$ or $SiO_xCl_y$ layer has built up over time, or whether the walls have been essentially stripped of oxide layers by a previous fluorine-containing plasma clean step.[1,9]

Qualitatively, it should be expected that the loss of Cl neutrals should lead to loss of $Cl^+$ ions. Variations in $Cl^+$ concentrations ($n_{Cl}^{+}$) due to varying Cl neutral recombination rates have been shown in simulations,[3] but to these authors' knowledge, this link has not been experimentally demonstrated and claims of constant or nearly constant plasma conditions in the presence of time varying neutral densities have been made.

We will show that *both* $n_{Cl}^{0}$ *and* $n_{Cl}^{+}$ can vary significantly during an etch run due to the chamber seasoning. Moreover, the plasma density variations due to chamber wall

condition also correlate strongly with real-time poly-Si etch rate changes, not merely average etch rate changes from run-to-run as previously shown. Choe et al. have previously shown that average Si etch rates in $Cl_2$ plasmas are controlled by the ion current to the wafer[10] and therefore are directly dependent upon $n_{Cl}^+$ densities. In this paper, we show the first real-time correlations between plasma density and Si etch rates. Further, we will show that using closed-loop feedback control to correct for plasma density transients flattens the real-time etch rate even though there is still variation in the $n_{Cl}^0$ concentration. Density variations due to chamber seasoning can be compensated using feedback control of the TCP plasma generation power. We will show that stabilizing the plasma density by varying TCP power also stabilizes poly-Si etch rate in $Cl_2$ plasmas, as well as $SiCl_4$ etch product levels in the exhaust within an etch run.

## II. EXPERIMENTAL METHODS

Four real-time monitoring systems were utilized for this project, to observe specific plasma, chemical, and wafer behaviors in the process chamber. The sensors used include: 1) a commercial Real-Time Spectroscopic Ellipsometer (RTSE) for *in situ* film evolution; 2) a custom-built impedance analyzer to determine plasma density, termed BroadBand RF; 3) a commercial Fourier Transform Infrared spectrometer (FTIR) for exhaust chemical monitoring; and 4) optical emission spectroscopy (OES) for chemical concentration in the plasma. Details of the OES and actinometry measurements, however, will be reserved for a future publication. The fundamental operating principles of the remaining three sensors are described next to better support data interpretation. Brief descriptions of the RIE testbed and control system are also included for reference.

4

All sensors described have data sampling frequencies in the ~1Hz-10Hz range, and all collected data are synchronously time stamped.

## A. High density plasma etch environment

The high density, low pressure RIE reactor platform for all experiments is a Lam Research TCP 9400SE. The upper chamber transformer coupled plasma (TCP) generation subsystem supplies 13.56 MHz radio frequency (rf) power through a matching network to a planar spiral coil. All experiments etch 150mm undoped poly-Si wafers, electrostatically chucked at 650V, with 100W bias rf forward power supplied to the lower electrode. Wafers are loaded through an entrance loadlock to prevent opening the process chamber to atmosphere. However, the wafers themselves may carry trace residual atmospheric water vapor on the surface when loaded. Process pressure is maintained at 10mT for all experiments using a variable position gate valve between the main chamber and the turbomolecular pump. Wafers are electrostatically clamped to chuck and even heat transfer is maintained by means of He backside cooling at a pressure of 8 Torr; with a typical He gas flow rate of 10-15sccm. Process gases enter the chamber via a gas distribution ring and flow rates are set with mass flow controllers. Chamber wall temperature is controlled at $45^{\circ}C$, and the lower electrode temperature is set to $60^{\circ}C$.

## B. Data acquisition and control system

A custom built, real-time data acquisition (DAQ) and control system, running in a LabVIEW™ environment, is wired in to compliment the original Lam Research I/O

boards on the tool.  In order to coordinate the multiple add-on and existing sensor systems, we required a framework to monitor, synchronize, trigger, and timestamp all pertinent data from the Lam tool and all external sensors.  In order to incorporate measured signals in a feedback control scheme, this new environment affords the capability of controlling the plasma input parameters in a real-time, deterministic manner, along with *in situ* data monitoring, chart display, and logging.  We chose a PC-based system running LabVIEW™ with data acquisition (DAQ) and General Purpose Instrument Bus (GPIB) boards from National Instruments for flexibility, ease of programming, and desired control rate performance.  A built-in TCP/IP data transfer protocol in the LabVIEW™ environment called DataSocket™ enabled easy transfer between sensor subsystems and the main control computer.  The resulting design records and actuates all relevant input and control signals at a sampling frequency of 4Hz for all experiments presented.

## C.  BroadBand RF resonance cavity density sensor

For chamber wall state and general plasma density state measurements, we employ a novel microwave cavity resonance sensor developed at the University of Michigan termed BroadBand RF.[11]  Previous work has been published describing the operation of the sensor.[12,13,14] In essence, the sensor monitors perturbations in cavity resonance peak frequencies as a function of plasma density and composition.  These peak power absorption frequencies are found to shift significantly depending on plasma conditions that affect density, such as chemical make-up, chamber wall state, and the plasma generation power.

Implementation of this sensing technique is straightforward. A small microwave antenna, housed in a protective quartz sheath, is inserted about 76 mm into the sidewall of the chamber as shown in Fig. 1. This is a minimally intrusive design which does not impinge upon the plasma or the etching characteristics at the wafer. The probe is not in contact with the plasma. Other density sensors, such as Langmuir probe methods, do not offer such unobtrusive advantages and therefore are considered prohibitive in an industrial setting.[15,16,17,18,19] By contrast, the BroadBand RF sensor is well suited for industrial applications since it offers little need for chamber modification and does not alter the process conditions or etch performance. In addition, BroadBand RF sensing compares favorably to Langmuir probe methods on a temporal scale. Both Langmuir probe voltage sweep measurements and BroadBand RF resonance peak measurements can produce reliable electron density data on millisecond timescales. However, BroadBand RF does not suffer from the heating or compensation issues associated with Langmuir probe methods and does not need metal probe contact in the plasma environment.[19,20] The BroadBand RF method is also easier to implement on commercial reactors than millimeter wave interferometry since it does not require two relatively large antennas on opposite sites of the chamber (with associated chamber windows).

**FIG. 1. BroadBand RF microwave probe in chamber.**

For the basic operating procedure, a low power (mW) microwave signal is launched into the chamber cavity, and the reflection coefficient $|\Gamma|$ is measured with a network analyzer

over a broad spectrum of frequencies. The resulting absorption spectra reveal resonance conditions at certain peak frequencies. Sample analyzer signatures are depicted for five different plasma conditions in Fig. 2; which are representative of the chamber conditions under study. The responses show two prominent absorption frequencies appear for this particular chamber chemistry and frequency range, designated $\omega_{n1}$ and $\omega_{n2}$.

**FIG. 2. Representative BroadBand peak frequency spectra for five different chamber conditions.**

This RF sensing technique is essentially plasma impedance spectroscopy, with the resonance modes of the chamber appearing as the high absorption peaks. The active microwave signal probes the natural resonance modes of the chamber, and the analyzer scans multiple frequencies for high absorption regions. In the data presented here, there are 201 frequencies in each scan, ranging from 0.5-3.0 GHz.

According to Slater's perturbation formula,[20] the BroadBand peak frequency position directly depends on the plasma density. To determine plasma density with a traditional cavity perturbation approach, assume the chamber volume geometric factors are idealized for analytic electric field forms. Assume conditions are such that the plasma is collisionless (e.g. $v_m << \omega_o$, where $v_m$ is the collision frequency and $\omega_o$ is the empty chamber resonance frequency). The plasma frequency $\omega_p$ is also much lower than the empty chamber resonance frequency, $\omega_p << \omega_o$. Under these conditions, frequency shifts, $\Delta\omega$, can be related to plasma frequency per,[21]

$$\frac{\Delta\omega}{\omega_0} = \frac{1}{2\omega_0^2} \frac{\iiint_r \omega_p^2 |E|^2 d^3r}{\iiint_r |E|^2 d^3r}.$$ (1)

Here, $E$ is the unperturbed resonance electric field, $\omega_0$ is the empty chamber resonance (no plasma ignited), $\omega_p$ is the plasma density, and the integrals are over the entire cylindrical cavity volume with radius $r$. (This formulation is true for all modes in the cavity, and our experiment assumes two dominant chamber modes, labeled $\omega_{n1}$ and $\omega_{n2}$.) Generally, knowing $\omega_0$ for the empty chamber (no plasma ignited) along with the nominal $E$ field from the idealized chamber geometry, measurement of the $\Delta\omega$ shift in resonance frequency in the presence of the plasma yields electron density for low density (collisionless) plasmas, due to the $\omega_p$ dependence on electron density, $n_e$, where

$$\omega_p^2 = \frac{n_e q^2}{m_e \varepsilon_0}.$$ (2)

Here, $q$ is fundamental charge, $\varepsilon_0$ the permittivity of vacuum, and $m_e$ the electron mass.

Regardless of the idealized features required for Slater's density analysis however, for a given resonant geometry at high plasma densities, small perturbations in resonance peak frequency are similarly observed in the presence of two *different* plasma conditions, not merely with and without plasma presence. These frequency shifts can still be attributed to changes in plasma density, which is the relevant point for the purposes of this paper.

It has been shown previously that peak absorption shifts to higher frequencies indicate comparatively higher electron density, and lower shifts indicate lower densities.[22] This

point can also be illustrated with a simple quasi-one-dimensional electromagnetic model using a Drude model of the plasma dielectric constant. We define the frequency dependent plasma dielectric constant, $\varepsilon_p(\omega)$, as

$$\varepsilon_p(\omega) = \varepsilon_0 \left[ 1 - \frac{\omega_p^2}{\omega(\omega - j\nu_m)} \right] \tag{3}$$

where $\omega$ is the driving frequency and $\nu_m$ is the collisional frequency. To simulate the reflection coefficient verses frequency, we model different capacitive loss paths and the associated impedance of each path, $Z_{pi}(j\omega)$, as an RLC circuit where

$$Z_{pi}(j\omega) = R + j\omega L + \frac{1}{j\omega C}. \tag{4}$$

Refer to Fig. 3 for a sample diagram of modeled capacitive loss paths.

**FIG. 3. Sample capacitive loss paths for 1D Drude model of reflection coefficient peaks.**

Each respective peak absorption frequency, $\omega_{ni}$, is then modeled as an RLC circuit resonance, given by

$$\omega_{ni} = \frac{1}{\sqrt{LC}}, \tag{5}$$

and the magnitude of the reflection coefficient, $|\Gamma(\omega)|$, is given by

$$|\Gamma| = \left| \frac{Z_o - Z_{tot}}{Z_o + Z_{tot}} \right|^2$$ (6)

where $Z_{tot}$ represents the total impedance of the sheath capacitance plus a given capacitive loss path impedance (e.g. to the wall or to the chuck), and $Z_0$ is the probe-to-plasma coupling impedance.

Simulated reflection coefficient spectra of the BroadBand simulation at different electron densities are shown in Fig. 4. First, this simple simulation illustrates that two sharp resonances can arise from a single plasma frequency but two significantly different ground-plane capacitances. In our present system, we speculate (but cannot prove) that these two peaks are due to distributed coupling to the chamber wall and TCP coil. Secondly, the simulation shows that several factors (particularly the collision rate $\nu_m$ and the coupling impedance $Z_0$) influence the overall shape of the reflection coefficient signal, but only plasma frequency (and therefore density), the volume of the plasma, and coupling capacitances are responsible for the peak resonance frequency positions. While we cannot completely rule-out the possibility that the sheath thicknesses (and thus coupling capacitances) vary somewhat during our experiments, we visually observe no changes in the volume or shape of the plasma during our experiments. Also, we have examined the ratio between the two BroadBand resonance peaks in our experiments, $(\omega_{n2}/\omega_{n1})$. If only the plasma density is changing (but not the geometric factors of path length and capacitance), we would expect this ratio to be constant. It is also possible that closely coupled changes in the sheath thicknesses would lead to changing peak frequencies under constant plasma density, but we have examined the $(\omega_{n2}/\omega_{n1})$ ratio for

11

the conditions of the experiments in this paper and found it to be nearly constant at 1.27 ±0.01 (even though the peak frequencies were shifting ~22%). This ratio of ($\omega_{n2}/\omega_{n1}$) holds constant under several different plasma conditions as well as when we changed wafers from a poly-Si covered surface to an $SiO_2$ covered surface. This strongly suggests that the chamber geometry is dictating the coupling capacitances and, thus, we attribute the experimentally observed changes in BroadBand peak frequency to plasma density changes when comparing different plasma conditions.

**FIG. 4. 1D Drude simulation of BroadBand absorption peaks modeled at five different electron densities. Peaks shift right at higher densities.**

Using a complete 3-dimensional electromagnetic modeling of the BroadBand RF measurement of a complete chamber loaded by a Drude dielectric model plasma to fit experimentally observed changes in peak shapes as well as frequency might also yield accurate time-resolved measurements of the collision rate and perhaps other plasma parameters.

**D. Real-time spectroscopic ellipsometry (RTSE)**

Poly-Si etch rates were monitored *in situ* using a rotating polarizer spectroscopic ellipsometer (a Sopra Real-Time Spectroscopic Ellipsometer – RTSE) with a prism-spectrometer/CCD detector system for high-speed measurements. Ellipsometry is a common optical technique for the characterization of thin films and for surface diagnostics, though its use in etch monitoring is less well documented.[23,24,25,26,27,28,29]

Several excellent references describe the principles, operation, and instrumentation of various ellipsometric systems,[30,31,32,33,34] both for single wavelength and multiple wavelength (spectral) systems. The RTSE system collected high resolution spectroscopic ellipsometry data over the spectral range of 300-780 nm with a data acquisition time of about 91 ms and a sampling time of about 180 ms. The fast data acquisition rate is needed so that the film thickness is nearly constant during the collection of one spectral sample (in our experiments < 0.5 nm of poly-Si is etched during an RTSE sample). This instrument provides an excellent method to quantitatively detect variations in etch rates. However, despite the high quality of the optical data, poly-Si is a notoriously difficult film to measure with sub-nm level absolute accuracy due to systematic errors introduced into the optically modeling by the presence of ~10-20 nm level surface roughness.[35] This modeling error produces oscillatory errors in the extracted film thicknesses and thus in the etch rates. These oscillations are evident in some of data presented in this paper, but do not affect our conclusions. Also, use of specular-mode spectroscopic ellipsometry and/or reflectometry on patterned wafers requires specialized test structures (typically gratings) and the use of computationally intensive vector diffraction theory.[36,37,38,39] Therefore, while it is an excellent monitor, *in situ* SE is not a good sensor for real-time feedback control of poly-Si etch rates.


**E. Fourier transform infrared spectroscopy (FTIR)**

An On-line Technologies INDUCT FTIR system was mounted to the turbo pump foreline of the main chamber pumping system for exhaust gas analysis. We measured the exhaust end of the chamber foreline to determine effluent species levels in the chamber.

Although the FTIR yielded several trace signals at the low foreline pressure (~100mT-200mT), we found the sensor to be particularly sensitive to monitoring two important effluent species in particular:  silicon tetrachloride ($SiCl_4$), which is a primary etch product when etching silicon with a $Cl_2$ plasma environment, and silicon tetrafluoride ($SiF_4$), a primary etch product in a fluorine containing environment.  The primary spectral lines recorded for these experiments are around 621 cm$^{-1}$ for $SiCl_4$ and 1022 cm$^{-1}$ for $SiF_4$, and the instrument is set to 0.5 wavenumber resolution.  Recording these molecular levels in real-time and comparing them with other density and etch rate measurements corroborated many of the results which will be shown later.  These measurements also helped determine the effect of chamber wall state and dynamic plasma variations on final etch performance.

## III.  EXPERIMENTAL RESULTS AND APPLICATIONS

Using the BroadBand absorption frequency data in real-time conjunction with independent RTSE rate data and FTIR and OES chemical data, we find that in addition to the reactive species concentration depending on wall condition, there are associated plasma density variations that can be attributed to the chamber wall state.  Moreover, these density variations can be compensated by feedback control of the TCP plasma generation power.  Demonstration and data to support these claims follows.

### A.  Ex. #1:  Real-time density control in $Cl_2$ plasma

This section shows that observed density transients in standard poly-Si etch $Cl_2$ plasmas are related to changes in the starting wall states and final etch performance results.  These

density variations are corrected using a real-time feedback controller that varies TCP power as a function of estimated density. To demonstrate such control compensation, three primary test conditions are considered: 1) seasoned chamber chlorine etches to establish steady state conditions; 2) open-loop control (i.e. uncontrolled) recovery from a non-seasoned chamber to observe transient behavior; and 3) closed-loop control recovery from a non-seasoned chamber to observe transient effect compensation. All three tests etch poly-Si wafers in the chamber.

Experiment 1 is the nominal etch. We first establish stable, seasoned etch conditions where all recorded signals are constant over long running $Cl_2$ plasmas, thus establishing "nominal" etch conditions. The stable, nominal chlorine etch chamber state is referred to as the Cl-prep condition. Establishing a nominal preparation step requires the recording of constant poly-Si etch rates, constant BroadBand peak frequencies, constant $SiCl_4$ FTIR signals, and constant Cl and Ar OES intensities. The nominal process recipe used for Cl-prep was 250W TCP, 100W bias, 10mT pressure, and 100sccm $Cl_2$ flow with 5% Ar.

Experiment 2 is the open-loop, disturbed etch. Once the Cl-prep condition is established as a baseline, the wall conditions are perturbed using a short (30sec) $C_2F_6$ plasma to alter the wall state of the chamber. The chamber state after a fluorine treatment is referred to as an F-prep condition. The F-prep recipe is 200W TCP, 40W Bias, 13mT pressure, and 100sccm $C_2F_6$. Following an F-prep, the second test involved a new poly-Si etch with identical chlorine plasma input conditions as used to establish the nominal etch. This is an uncontrolled, open-loop recovery of the chamber from F-prep back to Cl-prep. Sensor

signal changes over time due to the previous F-prep step are recorded. Observed transients for all sensors due to the F-prep starting wall condition were found to eventually stabilize back to steady state nominal Cl-prep conditions if the recovery plasma was allowed to run long enough, typically >300s.

Experiment 3 is the closed-loop, disturbed etch. The third test incorporated a PI feedback control algorithm in the system. As with the second test, a 30s F-prep plasma was performed in the chamber prior to the Cl recovery etch, so as to place the chamber in an unseasoned state. The chlorine etch recipe is then initiated on a poly-Si wafer. Now, however, the controller used BroadBand peak frequency (indicating plasma density) as the variable to be regulated, and TCP input power as the actuator. The target closed-loop setpoint frequency is the original peak absorption frequency recorded during the nominal Cl-prep. In this case, the target closed-loop frequency is set to $\omega_{n2}=1.650GHz$. As with the open-loop test, the etch proceeds for 60s; during which, etch product variables are measured for possible performance improvements. Variability in etch rate, BroadBand frequency position, $SiCl_4$ exhaust levels, and OES intensities were compared in real-time vs. the open-loop values measured from the second test. Values are also compared with nominal signals from the first test.

Figure 5(a) shows a real-time comparison between nominal etch rate in a stable Cl-prep chamber and the uncontrolled open-loop etch rate which started from an F-prep chamber. Figure 5(b) shows a similar comparison for the corresponding density indicator (the second BroadBand peak frequency $\omega_{n2}$). Note the significant drop in both etch rate and

plasma density at the start of the open-loop runs. The beginning etch rate shows about a 38% drop from its nominal point, while the BroadBand peak frequency drops by roughly 22%. However, since $n_e \propto \omega_n{}^2$, we have the relationship $\left( \dfrac{n_{e,start}}{n_{e,final}} \right) = \left( \dfrac{\omega_{n2,start}}{\omega_{n2,final}} \right)^2$ and therefore a 22% change in peak position corresponds to a roughly 39% change in density; the same change as the etch rate suppression. Clearly, the F-prep step to remove halogenated oxides from the chamber surfaces has a large effect on plasma density as well as plasma chemistry, and transients in these quantities due to the starting wall condition correlate to real-time etch rate.

**FIG. 5. Comparison of (a) nominal and open-loop etch rates and (b) BroadBand peak frequency nominal and open-loop position.**

In the 60s time allotted for the open-loop etch, neither BroadBand frequency nor the etch rate had sufficient time to recover to their respective nominal values. Tests show the recovery time back to nominal Cl-prep conditions with the nominal recipe takes ~5mins.

By contrast, Fig. 6(a) compares the closed-loop etch rate to the nominal etch rate in the top plot, while the corresponding $\omega_{n2}$ peak is compared in the lower plot. We see that the density recovery time is drastically reduced to ~5s and the corresponding real-time etch rate is also quickly leveled out.

**FIG. 6.  Comparison of (a) nominal and closed-loop etch rates and (b) BroadBand peak frequency nominal condition and under closed-loop control, starting from a perturbed chamber.**

Utilizing the FTIR system to measure etch product species in the foreline exhaust, we find similar behavior in the relative concentration of $SiCl_4$.  Figure 7 compares $SiCl_4$ levels for the same three etches.  Note the suppression of $SiCl_4$ early in the open-loop etch due to the loss of Cl species to the walls.  Conversely, the closed-loop etch compensates for the density loss to the walls with proportionally higher TCP power, and thus quickly raises the $SiCl_4$ level close to the nominal point.  The overall concentration is also more steady throughout the etch with closed-loop compensation.  $SiCl_4$ etch product levels return to the nominal point after 10-20s using feedback control, whereas the open loop recovery is unable to achieve nominal levels even after 60 s.

**FIG. 7.  Relative concentration of $SiCl_4$ etch product.**

We next plot in Fig. 8 the actuator signal, TCP power, to qualitatively see how the controller responds to the wall disturbance.  Note the sharp increase in TCP power at the start of the etch to compensate for the density losses to the walls.  The ion loss rate is highest for the clean wall condition at the start, as compared to the Cl-prep seasoned condition.  As oxychloride forms again on the walls, the Cl loss rate decreases, with a corresponding reduction in the TCP power. Eventually, the compensating power will

return to the open-loop nominal 250W setpoint.  By comparison, the open-loop TCP

power is set constant at 250W.

**FIG. 8.  TCP input power for open-loop & closed-loop experiments.**

We interpret the results of these experiments to mean that plasma density is significantly

altered by the chamber wall state, either because the recombination rate at the walls is

changing due to oxychloride buildup, or the electrical character of the dynamically

seasoned chamber walls alters the actual delivered power to the plasma; or possibly some

combination of both.  Regardless, maintaining a constant density corrects for these

transient effects.

We additionally performed Cl actinometry measurements during these experiments

monitoring the 822.2nm Cl emission line and the 750.4nm Ar line with 5% Ar in the gas

mixture.  Our results under the open-loop conditions with constant TCP power are very

consistent with the observations of Aydil et al.[1,7,9] and show $n_{Cl}^0$ variations due to the

wall state.  However, the Si etch rate more strongly correlates with the plasma density

variation (and thus presumably with the $n_{Cl}^+$ variation) as demonstrated in Fig. 5.  Further

quantitative interpretation of the actinometry data and $n_{Cl}^0$ neutral variation behavior will

be presented in detail in a future publication.[40]

**B. Ex. #2: Application to first wafer effect reduction**

The preceding section illustrated control of plasma density by TCP input power compensation over one run, in the presence of a wall-state disturbance. Another application of the density control technique is presented here over multiple wafers to demonstrate elimination of the so-called first wafer effect. This effect shows up as a performance loss in etch rate following chamber cleaning, wherein the first few wafers in a lot etch slower than subsequent wafers after a clean procedure. For pure $Cl_2$ etches, we find this lower etch rate can be corrected with feedback control, and the average etch rate for each wafer falls within much tighter tolerance limits.

For this second experiment, six total poly-Si etches are performed in succession. The first set of three etches is run in open-loop (i.e., with no controller), and the second set of three is run with closed-loop control as described in the preceding section. Prior to running, a nominal BroadBand frequency is established using a bare-Si wafer in a $Cl_2$ plasma. The steady state plasma input conditions are identical to those described in section A, and the resulting nominal BroadBand peak frequency after several minutes is found to be similar at $\omega_{n2}$=1.6625 GHz. This value is then used as the control setpoint for the BroadBand density measurement when performing closed-loop.

Undoped blanket poly-Si thickness measurements are made before and after each etch using a microscope-based spectral reflectometer – also called a spectrophotometer or "SP". An SP-style measurement is a common *ex situ* thickness technique practiced throughout the industry. For poly-Si measurements, the absolute accuracy of the SP is

affected by surface roughness issues (as is spectroscopic ellipsometry) but the optically estimated thickness does decrease monotonically with the actual film thickness. The repeatability of the instrument is within $\pm5\text{Å}$. Subtracting the before and after thickness measurements, we calculate the total etched material for each run and compare them.

Before each set of three etches is executed, a single $C_2F_6$ F-prep of the chamber is performed for 30s on a bare-Si wafer to clean material from the chamber sidewalls and top plate, leaving it in a fluorinated state. For the first experimental set, wafers 1, 2, and 3 are etched for 30s each in a $Cl_2$ plasma with no compensating control, and the resulting total etched material is recorded for each run. For the second experimental set, the chamber is once again cleaned with a $C_2F_6$ plasma F-prep, and three more wafers are processed for 30s in $Cl_2$. This second set, however, uses closed-loop compensation during each 30s etch to maintain the peak BroadBand frequency at the nominal $\omega_{n2}=1.6625$ GHz value for each run. Total etch depth for wafers 1, 2, and 3 are once again recorded for comparison with the first open-loop set.

Total etched material for the first open-loop set is plotted sequentially in Fig. 9(a). As expected from the real-time results of section A, the total etched material over a 30s process is found to increase for each wafer, which clearly demonstrates the common first wafer effect. The etch rate is increasing for each run as the wall seasons with oxychloride buildup and the recombination rate goes down. In just three wafers during standard open-loop conditions, the etch depth increases by $\sim150\text{Å}$ due to the dynamic wall interactions in the chamber.

**FIG. 9.  Etch depth following C$_2$F$_6$ cleans:  (a) open-loop and (b) closed-loop etches**

The results of the closed-loop set are shown in Fig. 9(b) for comparison.  The (max-min) difference is greatly reduced, by a factor of three, to ~50Å, vs. the same etches performed in open loop.  Although only three etches were performed for demonstration of the effect reduction, subsequent etches under closed-loop control would be expected to further improve the rate performance variation.

Since the walls continue to season and approach the nominal Cl$_2$-prep condition over time, the control action required to compensate the lower plasma density is expected to be reduced with each successive run.  Figure 10 shows the controller action (TCP power) for closed-loop runs 1, 2, and 3.  As expected, the magnitude of the TCP power required to maintain the nominal plasma density is smaller and smaller for each run.  Thus we would expect further runs to require smaller and smaller compensation for etch rate changes, therefore greatly improving the overall standard deviation compared to open-loop etches.

**FIG. 10.  Closed-loop control action after single C$_2$F$_6$ clean**

**C.  Ex. #3:  Application to etch depth variance reduction**

The previous section demonstrated the application of closed-loop density control to essentially eliminate the first wafer effect seen after chamber cleans.  This section

addresses another, more stringent, open-loop vs. closed-loop comparison which is known to be present in the IC manufacturing environment. For this demonstration we assume that, during process design, engineers are aware of the first wafer effect rate transient, and suppose that the resulting transient is repeatable after each clean. Due to the wall state variations, the only known and consistent chamber condition is that of the "cleaned" F-prep state. Therefore, in an effort to reduce etch depth and rate variance, each $Cl_2$ etch is preceded by a fluorine clean step to strip the walls back to the known state. So long as the total etch time is the same on each run, the total etched material will be consistent from run to run, even though the real-time etch rate is changing, because the rate of change is consistent for each run. This exact scenario is currently being advocated by equipment manufacturers for standard chlorine etches, using $SF_6$ as the fluorination cleaning gas.[7] We will next compare the etch depth variation obtained with this etch policy to that obtained with feedback control.

For this third experiment, we set up a comparison of two sets of five etches each, the first set running open-loop and the second using closed-loop density control. Prior to each etch, an empty chamber plasma clean is initiated using a standard $SF_6/Cl_2$ cleaning recipe provided in the Lam Research 9400SE Maintenance Manual. This recipe strips the chamber walls of oxide layers and leaves it in a known F-prep state, as is being advocated in industry. This F-prep cleaning plasma is run for 30s. Cleaning conditions are 700W TCP, 0W bias, 150sccm $SF_6$, 100sccm $Cl_2$, and 18mT process pressure.

23

We wish to target an etch depth of 2000Å on undoped poly-Si wafers for both open-loop and closed-loop cases. In an effort to make as close a comparison as possible, and not artificially bias the results, care was taken to establish an open-loop etch time which would consistently target 2000Å of etched material. This was accomplished by running several test wafers to determine an average etch rate during the main etch condition. Average etch rates were calculated by *ex situ* SP measurement of the film thickness before and after each etch, and dividing by the etch time. F-prep chamber cleans were performed prior to running each test wafer to establish a consistent average etch rate. Once a suitable average rate was determined, the total etch time was set so that a 2000Å target of etched material would be achieved in the open-loop case. The open-loop plasma input conditions for this experiment are 300W TCP, 50W bias, 10mT, 100sccm $Cl_2$, and 5sccm Ar. Under these conditions, following an F-prep clean, the desired etch time is found to be 64s to achieve a 2000Å etch depth.

As established previously, the closed-loop and nominal etch rates are significantly higher (>35%) than the corresponding open-loop etch rates after an F-prep chamber clean. The closed-loop etch rate, however, can be adjusted through choice of the BroadBand peak frequency setpoint. In the previous two experiments, we chose to set the closed-loop density at the same value as the nominal value, and therefore we achieved higher rates than in open loop. Here, we will instead choose a BroadBand frequency setpoint so as to achieve an average etch rate that is identical as possible to that of the open-loop etches.

The experiment is set up so that the only significant difference between the two sets of etches is that one applies constant TCP power and one adjusts TCP power so as to maintain a constant plasma density. Therefore, in determining the closed-loop etch time (and rate), we choose a peak frequency setpoint which is lower than the corresponding nominal point and yields an etch rate and etch time very close to the etch time required in open loop to achieve a 2000Å etch depth. Determining the etch time under closed-loop control is very simple because the real-time etch rate is now nearly constant (i.e., the real-time etch rate and the average rate determined from before and after thickness measurements are essentially the same). We determine that a setpoint frequency of $\omega_{n2}$=1.7125 GHz yields a total etch time of 62s required to etch 2000Å in closed-loop. As before, apart from the variable TCP input power, all plasma input conditions are the same for the closed-loop case: 50W bias, 10mT pressure, 100sccm $Cl_2$, and 5sccm Ar.

Figure 11(a) shows the total etched material in five open-loop etches in the upper plot, and five closed loop etches in the lower plot, Fig. 11(b). The open-loop etches have a (max-min) range of 72Å, when all five etches are run for the same amount of time and from a known starting chamber state using an $SF_6$ cleaned F-prep recipe for 30s. This technique clearly yields an improvement in the reduction of the first wafer effect when compared to plots such as Fig. 11 where the (max-min) was 150Å.

**FIG. 11.  2000Å etched material target for (a) open-loop & (b) closed-loop.**

However, even when starting from the same initially clean chamber state and running for similar times, the closed loop etches shown in Fig. 11(b) still demonstrate a larger improvement in the reduction of first wafer effect variance. The closed loop spread in the data is down to 48Å, which compares quite well with the min/max spread from the preceding section B experiments. More importantly, the $SF_6$ clean recipe step could be eliminated altogether and still yield the same results, thus saving an entire chamber preparation step and positively impacting Overall Equipment Efficiency (OEE).

Another important point to make regarding this data is the average etch depth value for each set. For the open loop runs, after 64s, the average etch depth is 1920Å, and none of the five attempts ever etched down to the 2000Å target. For the closed-loop etches, after 62s, the average etch depth is 2024Å, and two of the runs achieved almost exactly the 2000Å target. It could be argued that if the open-loop etches were allowed to run perhaps 2 seconds longer, then the open-loop average depth would be improved. However, such an argument belittles the difficulty stated earlier in obtaining a "correct" etch time in the open-loop case while the real-time etch rate is varying. The closed-loop case, on the other hand, had an easily obtained target etch time because the real-time etch rate and the average etch rate are essentially constant, and the success of that selected etch time is borne out in the final results. Moreover, significantly fewer test wafers were required to obtain the "correct" etch time for the closed-loop case than were needed in the open-loop case. This again will positively impact Overall Equipment Efficiency (OEE) by reducing both the need for chamber clean steps between wafers and the number of test wafers required to obtain proper processing times.

26

The evidence presented here strongly suggests that even in the most stringent comparison to open-loop etches, the closed-loop etch rate is more consistent from run to run when controlling for density variations due to wall state. It furthermore suggests that the transient real-time etch rate recovery in open-loop due to plasma cleaning before etching is not strictly consistent from run to run. Feedback control of density can further reduce the final etch depth variation by another 33%, and this improvement happens *with or without the additional plasma clean step*. Therefore, feedback control offers the potential to increase wafer throughput by eliminating the need for fluorine plasma cleaning steps between processes and still improve the overall etch consistency and performance. Furthermore, since the real-time etch rate is more constant from run to run, determining the desired etch time is significantly easier under feedback control, and targeted etch depths are more quickly obtained and consistently achieved.

### D. Effects of density control on profile development

Feedback control results discussed thus far pertain strictly to unpatterned blanket film wafers. We next explore the effects of density control on sidewall profile and overall pattern topography for silicon etching in $Cl_2$ plasmas.

The experimental setup is very similar to that of section A, where three etch conditions are compared. First, a nominal baseline etch is obtained for the profile development in a seasoned chamber in a $Cl_2$ environment. Second, the chamber wall-state is perturbed with a $C_2F_6$ cleaning step, and then the $Cl_2$ etch is allowed to proceed in an open-loop

27

manner.  Thirdly, the chamber is once again cleaned with $C_2F_6$ and the $Cl_2$ etch is initiated under closed-loop density control using the BroadBand RF peak frequency value achieved during the nominal etch as the closed-loop reference setpoint.  SEM (scanning electron microscope) cross-section images are used for profile comparison.

Test wafers for this work consisted of 50/50 duty cycle grating structures with 0.35μm lines and spaces.  A photoresist (PR) mask of the grating was imprinted over a 5000Å oxide layer.  An $SiO_2$ hardmask was generated using a $C_2F_6$ plasma to etch the pattern into the oxide, and the photoresist was then stripped away.  The resulting oxide hardmask pattern defines the grating for the silicon etches presented here.  The subsequent silicon etches used $Cl_2$ as the main etch plasma.  Note the SEM profile photos in Figs. 12-14 that follow still retain the $SiO_2$ hardmask at the top of each grating line.

Again, three etch experiments are performed: 1) a nominal seasoned etch; 2) an open-loop disturbed etch; and 3) a closed-loop disturbed etch.  For the first experiment where the chamber is in the Cl-prep state, the nominal chlorine main-etch condition is 250W TCP (upper electrode), 100W Bias (lower electrode), 10mT chamber pressure, 100sccm $Cl_2$, and 5sccm Ar for 100s plasma-on time.  The resulting cross sectional profile for this nominal etch is shown in Fig. 12.  We use this nominal profile etch as the reference point to determine the effects of feedback control on overall profile.  The micro-trench features themselves are not as important as how the shapes are affected by wall seasoning and feedback control.  Rather, the features changes under different chamber starting

conditions is the relevant point. This profile is used as a representative comparison with profiles from F-prep starting conditions.

We select the relevant parameterization for this profile to include an overall etch depth of 1.66μm (includes both $SiO_2$ mask + Si depth), a Si etch depth of 960nm, a micro-trench feature height of 193nm, and a CD of 830nm at the base of the feature. These results, along with open-loop and closed-loop disturbance etches, are summarized in Table I,.

**FIG. 12. Si profile after 100s $Cl_2$ nominal etch in seasoned chamber.**

For the second experiment, the chamber walls are first perturbed with a 30s $C_2F_6$ recipe of 200W TCP, 40W Bias, 13mT, and 100sccm $C_2F_6$ before starting the silicon etch. The identical $Cl_2$ etch as the nominal recipe is then performed in open-loop using set input conditions for 100s. Comparisons with the nominal profile are made to determine if the fluorine preparation step had any effect on resultant profile. The final cross-sectional SEM image for this test is shown Fig. 13.

Parameterization of this profile shows a smaller overall profile height of 1.59μm and a smaller Si etch depth of 871nm compared to the nominal etch profile. These results are consistent with the findings of section A for blanket etch rates, where the real-time etch rate is seen to be reduced due to fluorine treatment. The overall micro-trench height is comparable to the nominal feature height at 189nm, and the base CD is essentially the

29

same at 830nm.  That is to say, the profile shape is largely unaffected by the fluorine disturbance, and only the overall etch rate is reduced, leading to a smaller etch depth.

**FIG. 13.  Si profile after 100s $Cl_2$ open-loop etch following $C_2F_6$ clean.**

The third etch experiment prepares the chamber once again in an identical fashion as in the open-loop case, using a 30s $C_2F_6$ chamber clean step before the main $Cl_2$ silicon etch. Now, however, the main etch proceeds at a fixed BroadBand peak absorption frequency, using TCP input power to compensate for decreased plasma density.  The resulting profile for this closed-loop etch experiment is shown in Fig. 14.  The total profile height $(SiO_2 + Si)$ has returned to the nominal condition at 1.66μm, and the Si etch depth is back to 962nm.  The micro-trench feature height is nearly identical to the nominal profile at 195nm, and the CD is once again about 830nm.  Again, tabulated results are compared for all three etches in Table I.  Comparing the profile in Fig. 14 to that of the nominal profile in Fig. 12, we may conclude that density feedback control has virtually no effect on feature topography, and only affects the overall etch depth; i.e. the real-time etch rate is maintained at the original seasoned condition.  While not necessarily improving overall etch profile results, we conclude that feedback density control shows no significant ill-effects on pattern topography.  All results are the same as that of the nominal etch.

**FIG. 14.  Si profile after 100s $Cl_2$ closed-loop etch following $C_2F_6$ clean.**

## IV. SUMMARY AND CONCLUSIONS

Several conclusions can be drawn from the work to date. First, chamber cleaning in fluorine is shown to produce significant transient effects in density, real-time etch rate, and effluent chemistry when fluorine chamber preparation is followed by chlorine plasmas. The root cause of these transients is assumed to be due to a dynamic oxychloride layer build-up process at the chamber walls.[1,4] In particular, a thin film of silicon oxychloride grows on the walls during $Cl_2$ plasma etches which alters the chemical and electrical state of the bulk plasma process. The dynamic nature of this buildup persists until it is thick enough to achieve a steady state creation/loss ratio, and the $Cl_2$ etch conditions become constant. Introducing a fluorine plasma after the oxychloride buildup will quickly strip away this thin layer and return the chamber to a nearly pristine state. The chamber seasoning alters recombination rates at the walls, which affects both the neutral species density in the discharge in agreement with earlier results,[1,2,6] as well as the new result of transient plasma density.

For material etch processes which are primarily ion density dependent, such as $Cl_2$ etching of undoped poly-Si, a feedback compensation loop can correct for the ion losses by manipulating the TCP input generation power. Such feedback control reduces variance in real-time etch rate, effluent chemistry, and density. Etches using this feedback control method are shown to reduce variability in final etch depth even when compared to etch depth variations with fluorine clean steps in between each process wafer. Such a feedback control method significantly reduces the first wafer effect in chlorine processes following fluorine cleaning steps or preventative maintenance cleans

31

(PM's).   Finally, there is evidence that density feedback control shows no negative impact on final profile results when maintaining higher densities throughout the etch.

Overall, density feedback control with TCP power compensation has been demonstrated to significantly reduce variations in plasma processes where density disturbances exist. The primary measurement tool for these results, the BroadBand RF monitor, is a non-intrusive sensing device which does not come in contact with the plasma and does not alter process conditions in its presence.  It is an extremely stable, reproducible sensor and is much easier to implement than other plasma density sensors. These results have been demonstrated on a widely used and commercially available tool using process recipes typical in the industry.   Therefore direct application of the technique to industrially relevant settings is promising.  Further improvements in the control of the etch process could be expected if the plasma density control (via the BroadBand sensor) were combined with induced bias voltage control (a technique which was not available on our equipment).[41,42] In our experiments, we believe that the ion density was the dominant factor controlling the ion flux to the wafer. In other gas chemistries and/or operating regimes, it is quite possible that ion density would strongly influence the induced bias voltage (under constant bias power) and that feedback control of the bias supply would be needed as well. This could be accomplished with a separate SISO control loop but is possible that a coupled 2-in (TCP power & bias power)/2-out (plasma density-Broadband & $V_{bias}$) MIMO contoller would offer speed and stability advantages as our group saw in earlier work on coupled neutral density control/$V_{bias}$ control in a capacitive-mode reactor.[43]

32

**TABLE I. Profile parameters and etch control conditions**

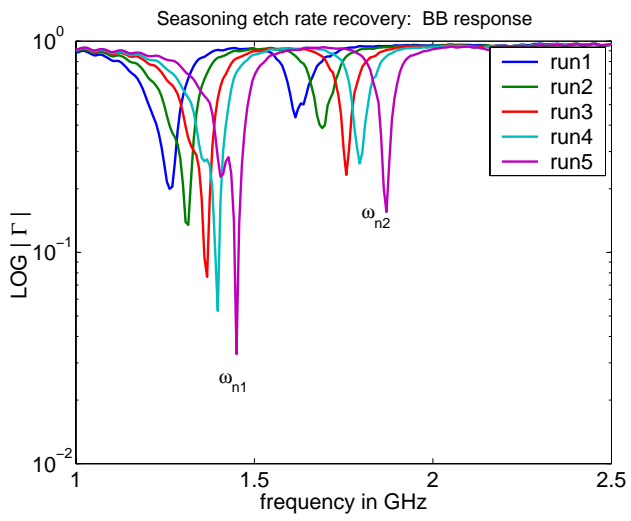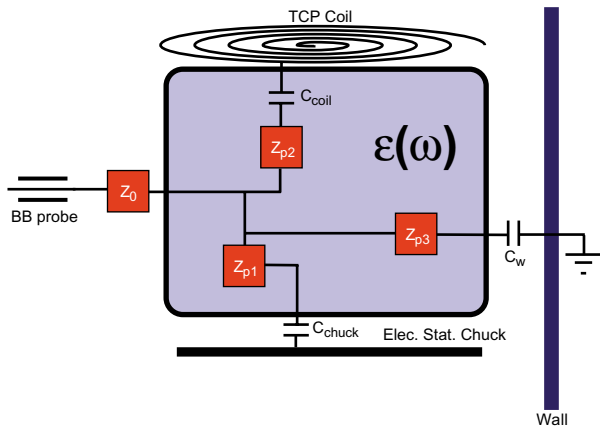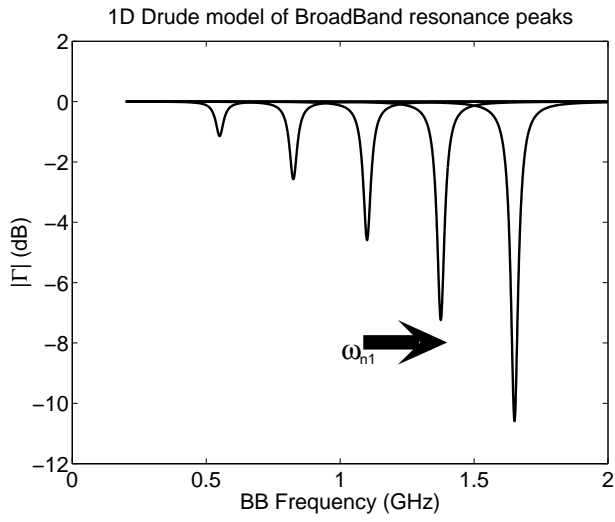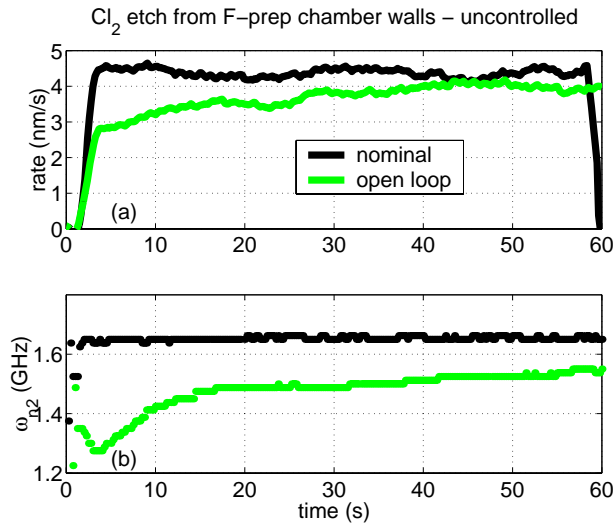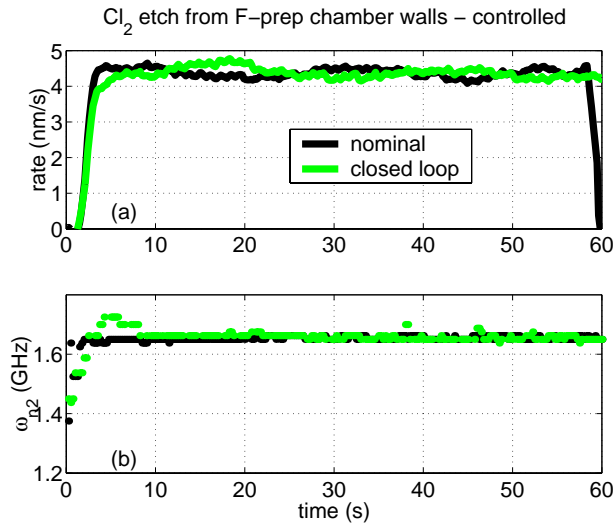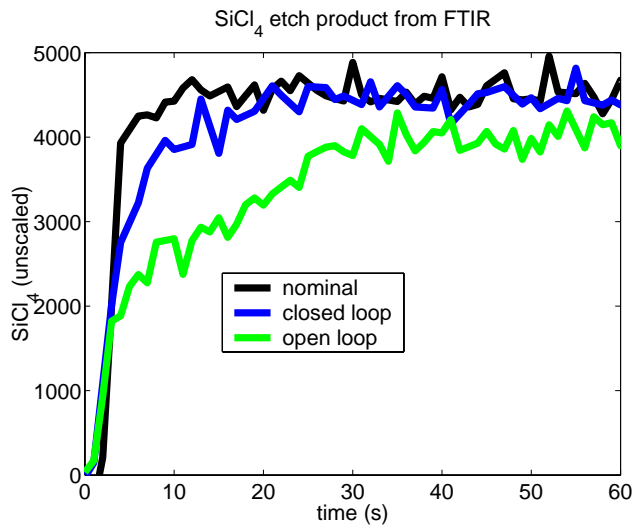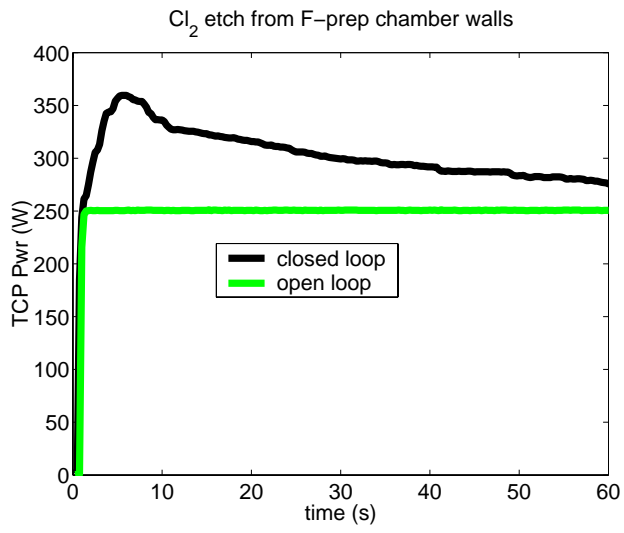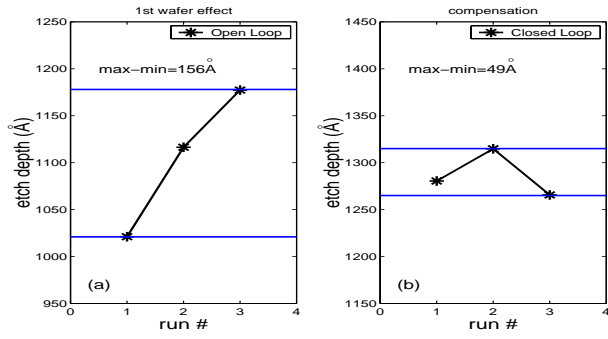|  | Si + $SiO_2$ depth | Si etch depth | Feature height | CD |
|---|---|---|---|---|
| Nominal | 1.66μm | 960nm | 193nm | 830nm |
| Open-Loop | 1.59μm | 871nm | 189nm | 830nm |
| Closed-Loop | 1.66μm | 962nm | 195nm | 830nm |
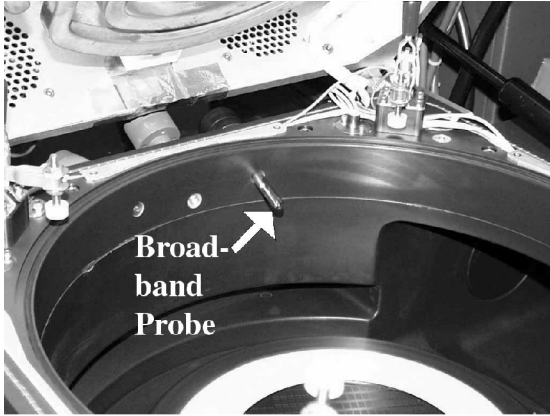
Figure 1, Klimecky, JVSTA

Figure 2, Klimecky, JVSTA

Figure 3, Klimecky, JVSTA

Figure 4, Klimecky, JVSTA

Cl$_2$ etch from F−prep chamber walls − uncontrolled

(a)

nominal
open loop

rate (nm/s)

(b)

$\omega_{n2}$ (GHz)

time (s)

Figure 5, Klimecky, JVSTA

38

Figure 6, Klimecky, JVSTA

SiCl$_4$ etch product from FTIR

Figure 7, Klimecky, JVSTA

Figure 8, Klimecky, JVSTA

Figure 9, Klimecky, JVSTA
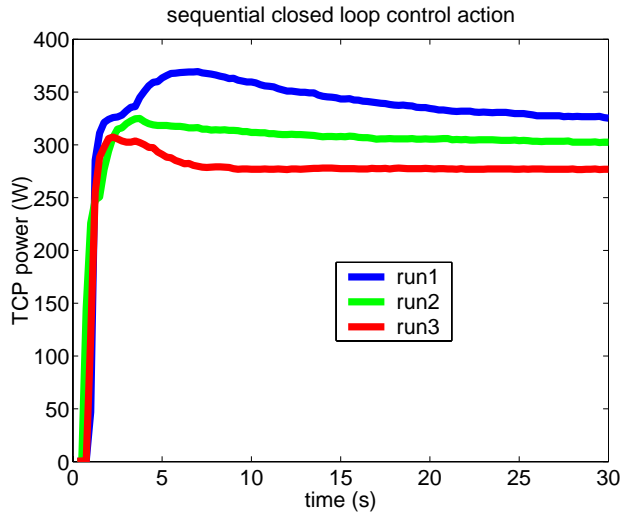
Figure 10, Klimecky, JVSTA
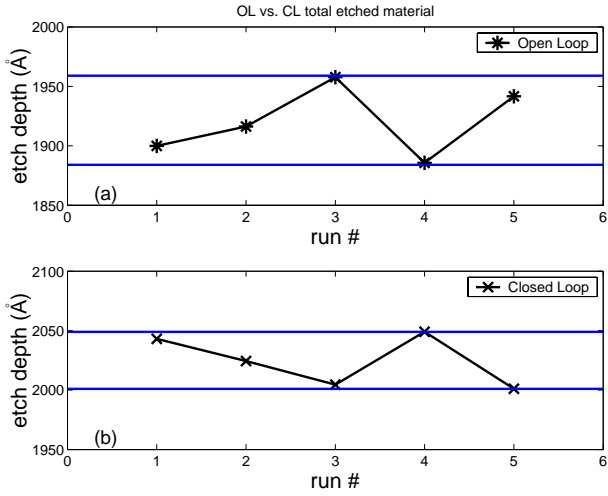
Figure 11, Klimecky, JVSTA
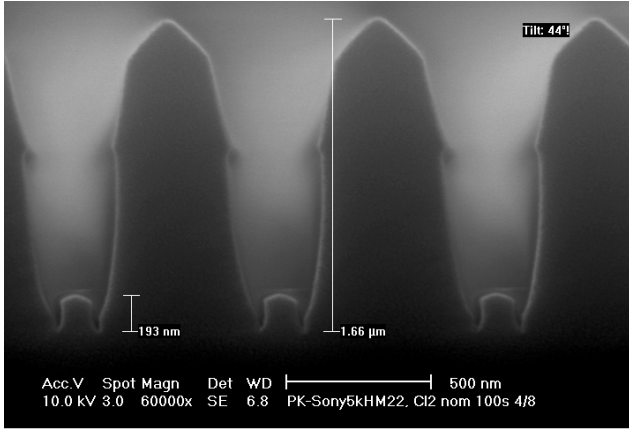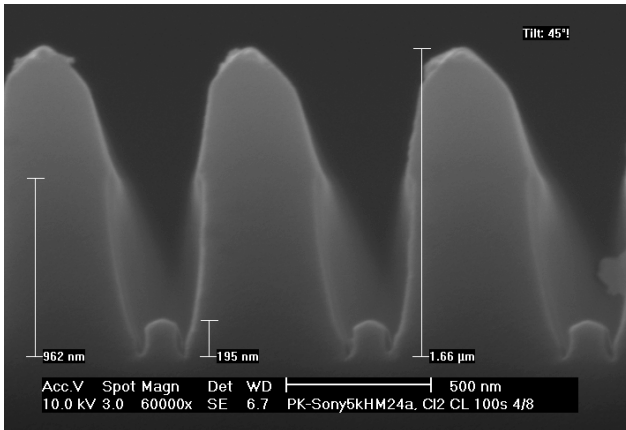
Figure 12, Klimecky, JVSTA
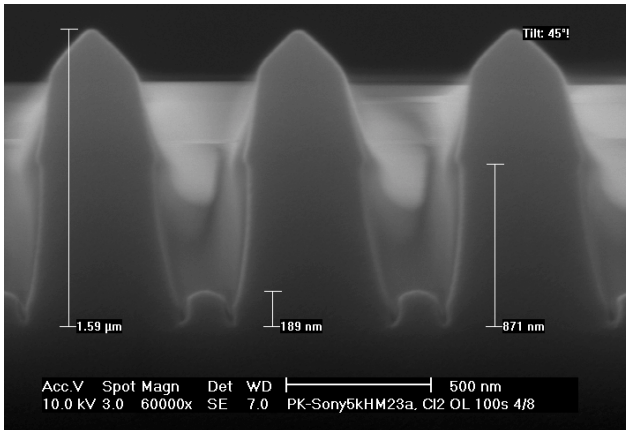
Figure 13, Klimecky, JVSTA

Figure 14, Klimecky, JVSTA

[1]  S. J. Ullal, A. R. Godfrey, E. Edelberg, L. Braly, V. Vahedi, and E. S. Aydil,  J. Vac. Sci. Technol. A **20**, 43 (2001)

[2]  V. M. Donnelly,  J. Vac. Sci. Technol. A **14**, 1076 (1996).

[3]  G. I. Font, I. D. Boyd, and J. Balakrishnan,  J. Vac. Sci. Technol. A **16**, 2057 (1998).

[4]  G. Zau and H. H. Sawin,  J. Electrochem. Soc. **139**, 250 (1992).

[5]  A. J. Watts and W. J. Varhue,  Appl. Phys. Lett. **61**, 549 (1992).

[6]  M. Malyshev and V. M. Donnelly,  J. Appl. Phys. **88**, 6207 (2000).

[7]  S. J. Ullal, H. Singh, J. Daugherty, V. Vahedi, and E. S. Aydil,  J. Vac. Sci. Technol. A **20**, 1195 (2002).

8  S. Xu, Z. Sun, X. Qian, J. Holland, and D. Podlesnik,  J. Vac. Sci. Technol. B **19**, 166 (2001).

9  S. J. Ullal, H. Singh, V. Vahedi, and E. S. Aydil,  J. Vac. Sci. Technol. A **20**, 499 (2002).

10  J. Y. Choe, I. P. Herman, and V. M. Donnelly,  J. Vac. Sci. Technol. A **15**, 3024 (1997).

11  C. Garvin, B. E. Gilchrist, D. S. Grimard, and J. W. Grizzle,  J. Vac. Sci. Technol. A **16**, 595 (1998).

12  C. Garvin, D. S. Grimard, and J. W. Grizzle, Char. & Metrology for ULSI Tech. **449**, 442 (1998).

13  C. Garvin, D. S. Grimard, and J. W. Grizzle, 195th Electrochemical Society Meeting, Seattle, WA, 256, (1999). The Electrochemical Society, Inc., (1999).

14  C. Garvin, D. S. Grimard, and J. W. Grizzle,  J. Vac. Sci. Technol. A **17**, 1377 (1999).

15  M. A. Lieberman and A. J. Lichtenberg, *Principles of plasma discharges and materials processing*, **1**st edition (John Wiley & Sons, Inc., New York, 1994), Vol. **1**, Chap. 6, p.172.

16  J. D. Swift and M. J.R. Schwar, *Electrical Probes for Plasma Diagnostics*, **1**st edition (Iliffe, American Elsevier, London, UK, 1969)

17  V. A. Godyak, R. B. Piejak, and B. M. Alexandrovich, Plasma Sources Sci. Technol. **1**, 36 (1992).

18  J. L. Kleber and L. J. Overzet, Plasma Sources Sci. Technol. **8**, 534 (1999).

[19] N. Hershkowitz, *Plasma Diagnostics-Discharge Parameters and Chemistry*, **1**st edition (Academic, New York, 1989), Vol. **1**, p.113-183.

[20] J. C. Slater, Rev. Mod. Phys. **18**, 441 (1946).

[21] M. Haverlag, G. M. Kroeson, T. H. Bisschops, and F. J. Dehoog, Plasma chemistry & plasma processing **11**, 357 (1991).

[22] P. I. Klimecky and C. Garvin, AEC/APC XII Symposium , Lake Tahoe, NV, (2000).

[23] M. Haverlag and G. S. Oehrlein, J. Vac. Sci. Technol. B **10**, 2412 (1992).

[24] H. L. Maynard and N. Hershkowitz, J. Vac. Sci. Technol. B **13**, 848 (1995).

[25] H. L. Maynard, A. N. Layadi, and J.T. C. Lee, J. Vac. Sci. Technol. B **15**, 109 (1997).

[26] N. Blayo, R. A. Cirelli, F. P. Klemens, and J.T. C. Lee, J. Opt. Soc. Am. A **12**, 591 (1995).

[27] S. Vallon, O. Joubert, L. Vallier, F. Ferrieu, B. Drevillion, and N. Blayo, J. Vac. Sci. Technol. A **15**, 865 (1997).

[28] H. T. Huang, W. Kong, and F. L. Terry, Jr., Appl. Phys. Lett. **78**, 3983 (2001).

[29] H. T. Huang, J. W. Lee, P. I. Klimecky, P. P. Khargonekar, and F. L. Terry, Jr., AEC/APC XIII Symposium, Banff, Alberta, Canada, (2001).

[30] R. M.A. Azzam and N. M. Bashara, *Ellipsometry and Polerized Light*, **2nd** edition (North Holland Personal Library, Amsterdam, 1987), Vol. **1**, p.1.

[31] D. D. Aspnes and A. A. Studna, Appl. Opt. **14**, 220 (1975).

[32] R. W. Collins, Rev. Sci. Instrum. **61**, 2029 (1990).

[33] G. Zalczer, Rev. Sci. Instrum. **59**, 2020 (1988).

[34]  G. E. Jellison, Jr.,  Thin Solid Films **1**, 416 (1993).

[35]  T E Benson, A Ramamoorthy, L I Kamlet, and F L Terry, Jr., Thin Sol. Films **313-4**, 177 (1998).

[36]  M. E. Lee, C. Galarza, W. Kong, W. Sun, and F. L. Terry, Jr., AIP Conf. Proc. **449**, 331 (1998).

[37]  B. S. Stutzman, H. T. Huang, and F. L. Terry, Jr., J. Vac. Sic. Technol. **B 16**, 2785 (2000).

[38]  H. T. Huang, W. Kong, and F. L. Terry, Jr., Appl. Phys. Lett. **78**, 3983 (2001).

[39]  N Xinhui, N Jakatdar, J. Bao, and C. J. Spanos, IEEE Trans. Semic. Manuf. **14**, 97 (2001).

[40] paper under preparation for submission to J. Vac. Sci. Technol. A.

[41]  R. Patrick, S. Baldwin, and N. Williams, J. Vac. Sci. Technol. **A18**, 405 (2000).

[42]  S. C. Lai, C. H. Cheng, C. Lin, and C. H. Tsai, IEEE Intl. Conf. on Plasma Sci., Las Vegas, NV, 476, (2001).

[43]  B. A. Rashap, M. E. Elta, H. Etemad, J. P. Fournier, J. S. Freudenberg, M. D. Giles, J. W. Grizzle, P. T. Kabamba, P. P. Khargonekar, S. Lafortune, J. R. Moyne, D. Teneketzis, and F. L. Terry, Jr., IEEE Trans. Semicond. Manuf. **8**, 286 (1995).